

Designing New Kinase Inhibitor Derivatives as Therapeutics Against Common Complex Diseases: Structural Basis of Microtubule Affinity-Regulating Kinase 4 (MARK4) Inhibition

Farha Naz,¹ Mohd. Shahbaaz,² Krishna Bisetty,² Asimul Islam,¹
Faizan Ahmad,¹ and Md. Imtaiyaz Hassan¹

Abstract

Drug development for common complex diseases is in need of new molecular entities and actionable drug targets. MAP/microtubule affinity-regulating kinase 4 (MARK4) is associated with numerous diseases such as neurodegenerative disorders, obesity, cancer, and type 2 diabetes. Understanding the structural basis of ligands' (inhibitors) and substrates' binding to MARK4 is crucial to design new kinase inhibitors for therapeutic purposes. This study reports new observations on docking three well-known kinase inhibitors in the kinase domain of MARK4 variants and the calculated binding affinity. These variants of MARK4 are named as MARK4-F1 (59N-terminal residues along with kinase domain) and MARK4-F2 (kinase domain of MARK4). We additionally performed molecular dynamics (MD) simulation and fluorescence binding studies to calculate the actual binding affinity of kinase inhibitors, BX-912, BX-795, and OTSSP167 (hydrochloride) for the MARK4. Docking analyses revealed that ligands bind in the large hydrophobic cavity of the kinase domain of MARK4 through several hydrophobic and hydrogen-bonded interactions. Simulations suggested that OTSSP167 (hydrochloride) is forming a stable complex, and hence the best inhibitor of MARK4. Intrinsic fluorescence of MARK4 was significantly quenched by addition of ligands, indicating their potential binding to MARK4. A lower K_D value of MARK4 with OTSSP167 (hydrochloride) suggested that it is a better interacting partner than BX-912 and BX-795. These data form a basis for designing novel and potent OTSSP167 (hydrochloride) derivatives as therapeutic candidates against common complex diseases. The inhibitors designed as such might possibly suppress the growth of tumor-forming cells and be potentially applied for treatment of a wide range of human cancers as well.

Introduction

DRUG DEVELOPMENT FOR COMMON COMPLEX DISEASES in ways that inform personalized medicine is in need of new molecular entities and drug targets that are actionable (Dimitrakopoulou et al., 2014; Lewis et al., 2014). In this connection, MAP/microtubule affinity-regulating kinase 4 (MARK4) is a member of serine/threonine kinases family and phosphorylates microtubule associated proteins (MAPs) on their microtubule binding domain, which leads to the disruption of their attachment with microtubules and change their dynamics.

MARK4 also phosphorylates Tau protein, which is directly associated with Alzheimer's disease (Drewes et al., 1995).

MARK4 is a mammalian homolog of PAR-1 (partition-defective 1), KIN1, and is involved in the regulation of various cellular events (Drewes et al., 1997; Kempfues 2000). MARK has four isoforms (MARK1–4) (Drewes et al., 1995; Illenberger et al., 1996; Trinczek et al., 2004). They represent a similar structural organization; one N-terminal header, a kinase domain, a ubiquitin associated (UBA) domain, a spacer region, and a kinase associated (KA1) domain (Bright et al., 2009; Marx et al., 2010; Timm et al., 2008).

MARK4 is predominantly expressed in brain followed by testis and lungs. It exists in two splice variants namely MARK4L and MARK4S (Trinczek et al., 2004; Tang et al., 2012). It is directly associated with many diseases such as neurodegenerative diseases, diabetes, and varying types of

¹Center for Interdisciplinary Research in Basic Sciences, Jamia Millia Islamia, Jamia Nagar, New Delhi, India.

²Department of Chemistry, Durban University of Technology, Durban, South Africa.

cancer. MARK4L is upregulated in metastatic breast carcinomas, hepatocellular carcinomas (Kato et al., 2001) and glioma (Magnani et al., 2011). MARK4 also acts as a negative regulator of mTORC1, which plays a role in Wnt signaling in prostate cancer.

All these studies suggested MARK4 as a potent target for cancer and other related diseases (Conrad et al., 2009; Gabrovska et al., 2012; Li and Guan 2013). Ablation of MARK4 significantly improved glucose homeostasis by up-regulating the activity and expression of AMPK kinase in key metabolic tissues (Sun et al., 2012), suggesting that development of MARK4 inhibitors may provide a better choice for the treatment for obesity and related metabolic complications, including type 2 diabetes (Sun et al., 2012).

The kinase inhibitors BX-912 and BX-795 are actually potent ATP-competitive inhibitors of 3-phosphoinositide-dependent protein kinase 1 (PDK1) (Feldman et al., 2005). PDK1 is a serine-threonine kinase that phosphorylates and activates a range of other kinases, including protein kinase (PK) B, PKA, and certain isoforms of PKC (Peifer and Alessi, 2008). They have been used to evaluate the role of PDK1 in kinase activation and cell survival (Kloo et al., 2011; Mashukova et al., 2012; Shibata et al., 2013). BX-795 also inhibits ERK8, MAPK-interacting kinase 2, Aurora B, Aurora C, MAP/ microtubule affinity-regulating kinase 1-4, TNF receptor associated factor-associated NF- κ B activator-binding kinase1, I κ B kinase ϵ , and additional kinases (Bain et al., 2007; Clark et al., 2009; Tamguney et al., 2008).

The OTSSP167 is a potent inhibitor of maternal embryonic leucine zipper kinase (MELK) (Chung et al., 2012). MELK is a serine-threonine kinase that regulates signaling central to cell cycling, stem cell renewal, apoptosis, and other cellular processes (Jiang and Zhang, 2013). MELK is overexpressed in some forms of cancer, particularly those with aggressive undifferentiated tumors (Gray et al., 2005; Joshi et al., 2013; Nakano et al., 2011). OTSSP167 suppresses the growth of diverse cancer cell lines at low nanomolar concentrations (Chung et al., 2012). It also blocks the phosphorylation of MELK-specific substrates and reduces the ability of MCF-7 breast cancer cells to invade and form spheroids in Matrigel (Chung et al., 2012).

As a strategy, docking of ligand with the protein has been used widely for the binding study between them. It also helps in knowing the application of ligands towards drug design (Hassan et al., 2007a, 2007b; Thakur and Hassan 2011; Thakur et al., 2013; Singh et al., 2014). Furthermore, fluorescence binding studies provide an insight into interaction of ligands to the protein (receptor).

Protein kinases play critical roles in growth signaling pathways in cancer cells (Brognard and Hunter, 2011). Its ATP-binding pocket has been considered as an ideal target for pharmacological therapy, and any differences in the residues of ATP-binding cavity confer selectivity of kinase inhibitors against a specific kinase (Yesilkanal and Rosner, 2014). For these reasons, protein kinases are considered as attractive therapeutic targets of anti-cancer drugs (Cowan-Jacob et al., 2009; Zhang et al., 2009).

MARK4 is also considered as a potential drug target for many life-threatening diseases such as cancer, Alzheimer's, diet-induced obesity, many metabolic disorders, and type 2 diabetes. Hence, there is a need for the designing of new therapeutic strategies for effective treatment of MARK4

associated diseases. Here, we expressed two variants of MARK4 named as MARK4-F1 (59 N-terminal residues along with kinase domain) and MARK4-F2 (kinase domain) and studied their biophysical properties (Naz et al., 2014, 2015b). We have chosen three known kinase inhibitors (BX-912, BX-795, and OTSSP167) and performed docking and MD simulation studies to see the structural basis of MARK4-ligand interactions. We further validated the binding affinity of these ligands to the MARK4 experimentally using fluorescence binding studies.

Materials and Methods

NaCl, EDTA, and other chemicals and reagents were bought from Merck (India). DNA preparation kits, ampicillin, kanamycin, monoclonal anti-His antibody, dialysis tubing, Luria broth, and Luria agar were bought from the Sigma Chemical Co. (St. Louis, USA). Ni-HF column was purchased from GE Healthcare (GE Healthcare Life Sciences, Uppsala, Sweden). Syringe filter of 0.22 μ was purchased from Millipore Corporation (USA). All chemicals and reagents were of analytical grade.

Structure prediction and validation

Three-dimensional (3-D) structures of MARK4-F1 and MARK4-F2 were predicted by homology modeling techniques present in the MODELLER server (Eswar et al., 2006). Templates were identified using PSI-BLAST (Altschul et al., 1990) module of Discovery Studio (DS) 3.5. Both F1 and F2 showed similarities with the crystal structure of MARK3 (PDB ID-3FE3) with a sequence identity of 90%. Template and query sequences were aligned, and structures of both the variants were predicted using the MODELLER by satisfying the spatial restraints. The energy minimization and optimizations of the predicted models were performed using DS modules CHARMM-22 force-field parameter (Hirashima and Huang, 2008). Side chain refinement of predicted models was done using side chain refinement protocol of MODELLER on Discovery studio 4.0.

The stereochemistries of the predicted models were analyzed using PROCHECK (Laskowski et al., 1996). PROCHECK analyzes residue-by-residue geometry and overall structure of protein and validates the stereochemical quality of a predicted models. MARK4-F1 showed 97.4% of the residues in the allowed regions of the Ramachandran plots, while for MARK4-F2 it was 98.7%. Hence, the stereochemistry of the predicted models were acceptable. Furthermore, ProQ was used to predict the correctness and quality of model structures (Wallner and Elofsson, 2003). The estimated quality score for MARK4-F1 was 5.358 and that for MARK4-F2 was 5.850. These estimates indicate the reliability of the predicted models. The final energy minimized and well validated models were taken for further study.

Molecular docking

Modeled structures of both MARK4-F1 and MARK4-F2 were used for docking studies with the kinase inhibitors using AutoDock 4.0 package (Morris et al., 2009). The AutoDock utilizes the combination of a free energy based empirical force-field along with Lamarckian Genetic Algorithm to

predict the bound conformations (Morris et al., 2009). The grid dimensions of $85 \times 85 \times 85$ Å were assigned using the AutoGrid module with grid spacing of 0.375 Å. The Lamarckian genetic algorithm was used with the default parameters. Around 100 conformations were generated that were clustered according to the RMSD tolerance of 2.0 Å.

Top 10 conformations were rescored using DrugScoreX server (Neudert and Klebe, 2011) and selected for MD simulation on the basis of consensus of the observed parameters. The docked complexes were optimized and validated using modules present in the “Receptor-Ligand Interactions” section of Discovery Studio 4.0 (BIOVIA 2013). Furthermore, docked complexes were minimized using CHARMM force-field (Vanommeslaeghe et al., 2010). Top 3 inhibitors were selected for MD simulation studies.

MD simulations

A set of six ligand docked complexes of MARK4-F1 and MARK4-F2 were selected on the basis of generated parameters (illustrated in Table 1). These docked complexes were subjected to MD simulations using GROMACS (Pronk et al., 2013) (version 4.6.5, installed on the CHPC server that provides 15 nodes with 8 cores per node of space for computation). The topologies of both MARK4-F1 and MARK4-F2 were generated using GROMOS96 53a6 force-field (Oostenbrink et al., 2004).

Because of unavailability of force-field parameters for drug-like molecules in the GROMACS package, we used PRODRG server (Schuttelkopf and van Aalten 2004) to generate topologies and coordinate files for ligands. The complexes were immersed in SPC/E water model (Zielkiewicz, 2005) and energetically minimized using the steepest descent algorithm with a convergence criterion of $0.005 \text{ kcal mol}^{-1}$. The restraints were applied to the complexes before the equilibration phase. The equilibration phase was carried out under NVT (constant volume) and NPT (constant pressure) each for 100 ps time scale. The temperature of the system was maintained at 300 K using Berendsen weak coupling method in both ensemble conditions along with pressure which was maintained at 1 bar by utilizing Parrinello-Rahman barostat in constant pressure ensemble.

Finally, the MD production was carried using LINCS algorithm for each complex at 20 ns time scale. Results extracted from the trajectory files were utilized for the analyses of each complex behavior in the explicit water environment. The RMSD (root mean square deviations), H-bonds and distances between protein and ligands were analyzed.

Cloning, expression, and purification

Cloning, expression, and purification of both the variants of MARK4 (MARK4-F1 and MARK4-F2) were done using our optimized protocol (Siddique et al., 2014). Briefly, PCR amplification of MARK4-F1 and MARK4-F2 genes were done using designed primers, and they were ligated into pQE30 expression vector. Expression vector along with desired genes were transformed in *E. coli* M15 competent cells. Cultures were kept overnight at 16°C on incubator shaker after induction by isopropyl β -D-1-thiogalactopyranoside (IPTG). Proteins were extracted from inclusion bodies (IBs) from these cultures.

IBs were further dissolved in CAPS, NaCl, and N-laurylsarcosine buffer and used for protein purification using Ni-NTA column. Imidazole was used to elude the bound protein. The purity of purified protein was checked by sodium dodecyl sulfate polyacrylamide gel electrophoresis (SDS-PAGE). Molar absorption coefficient values of $31775 \text{ M}^{-1} \text{ cm}^{-1}$ for MARK4-F1 and $26150 \text{ M}^{-1} \text{ cm}^{-1}$ for MARK4-F2 at 280 nm were used to determine the protein concentrations (Pace et al., 1995). Activity of proteins was checked by ATPase assay where formation of ^{32}P from $[\gamma\text{-}^{32}\text{P}]$ ATP catalyzed by MARK4-F1 and MARK4-F2 were assayed as described previously (Siddique et al., 2014).

Measurement of absorption spectra

Absorption spectra of all three selected ligands BX-795, BX-912, and OTSSP167 were taken in Shimadzu 1601 UV/Vis Spectrophotometer. An external refrigerated water bath was used to maintain the temperature of cell holders. $27 \mu\text{M}$, $10 \mu\text{M}$, and $9 \mu\text{M}$ of BX-795, BX-912, and OTSSP167, respectively, were taken for spectral measurements in wavelength range of 1100–200 nm. Spectral measurements were done three times at $25 \pm 0.1^\circ\text{C}$ using 1 cm path length cuvette.

Measurements of fluorescence spectra

All the fluorescence measurements were carried in Jasco spectrofluorometer (Model FP-6200) at $25 \pm 0.1^\circ\text{C}$ using 5 mm quartz cuvettes. Temperature of the spectrofluorometer was maintained by an external thermostated water circulator. Excitation wavelength was set at 280 nm, whereas emission spectra were recorded in the range 300–400 nm. Both BX-795 and BX-912 were dissolved in dimethyl formamide (DMF) and OTSSP167 (hydrochloride) was dissolved in dimethyl sulfoxide (DMSO) in a final concentration of 1 mg/mL. Two blanks (i) ligands were gradually added to the

TABLE 1. PARAMETERS GENERATED FROM MOLECULAR DOCKING SHOWING INTERACTION BEHAVIORS OF PROTEINS AND LIGANDS

S. No	Complex name	Selected docked pose	DrugScoreX scoring results	Free energy of binding (kcal/mol)	Ligand efficiency	vdW + Hbond + desolv energy (kcal/mol)	Intermolecular energy (kcal/mol)	Total internal energy (kcal/mol)	Torsional energy (kcal/mol)
1.	F1_BX-795	4	-84	-5.42	-0.16	-8.31	-8.1	-2.56	2.68
2.	F1_BX-912	1	-101	-5.51	-0.18	-7.01	-7.6	-2.96	2.09
3.	F1_OTSSP167	3	-91	-7.97	-0.24	-9.45	-10.06	-2.04	2.09
4.	F2_BX-795	7	-88	-5.63	-0.17	-8.45	-8.31	-2.82	2.68
5.	F2_BX-912	1	-84	-6.87	-0.23	-9.06	-8.95	-1.63	2.09
6.	F2_OTSSP167	2	-95	-7.91	-0.24	-9.95	-10.0	-2.15	2.09

buffer without protein and (ii) buffer to the protein solution. Titration was done by adding 0.5 μL (2.11 μM) of BX-795, 1 μL (1.06 μM) of BX-912, and 1 μL (0.95 μM) OTSSP167 (hydrochloride) to the 0.1 mg/mL of MARK4-F1 and MARK4-F2 solutions. Final spectrum was collected after subtracting corresponding blanks. For data analysis, an average of three independent experiments was taken.

Results

Molecular docking

Structure of ligands BX-795, BX-912, and OTSSP167 were generated by MARVINSKETCH and were used for

docking (Supplementary Fig. S1A, B, and C; supplementary material is available online at www.liebertpub.com/omi). Superimposed model structure of MARK-F1 and MARK4-F2 are shown along with active site (Supplementary Fig. S2). Conformations of docked ligands with MARK4-F1 and MARK4-F2 are shown in Figures 1 and 2, respectively. Dali server (Holm and Rosenstrom, 2010) was used to identify the structural homologs for both the proteins.

On the basis of structural comparisons with the templates and the information available in the literature, we identified residues that may be the part of their active sites. Furthermore, the annotations of active sites of both proteins were validated on the basis of outputs obtained from COACH

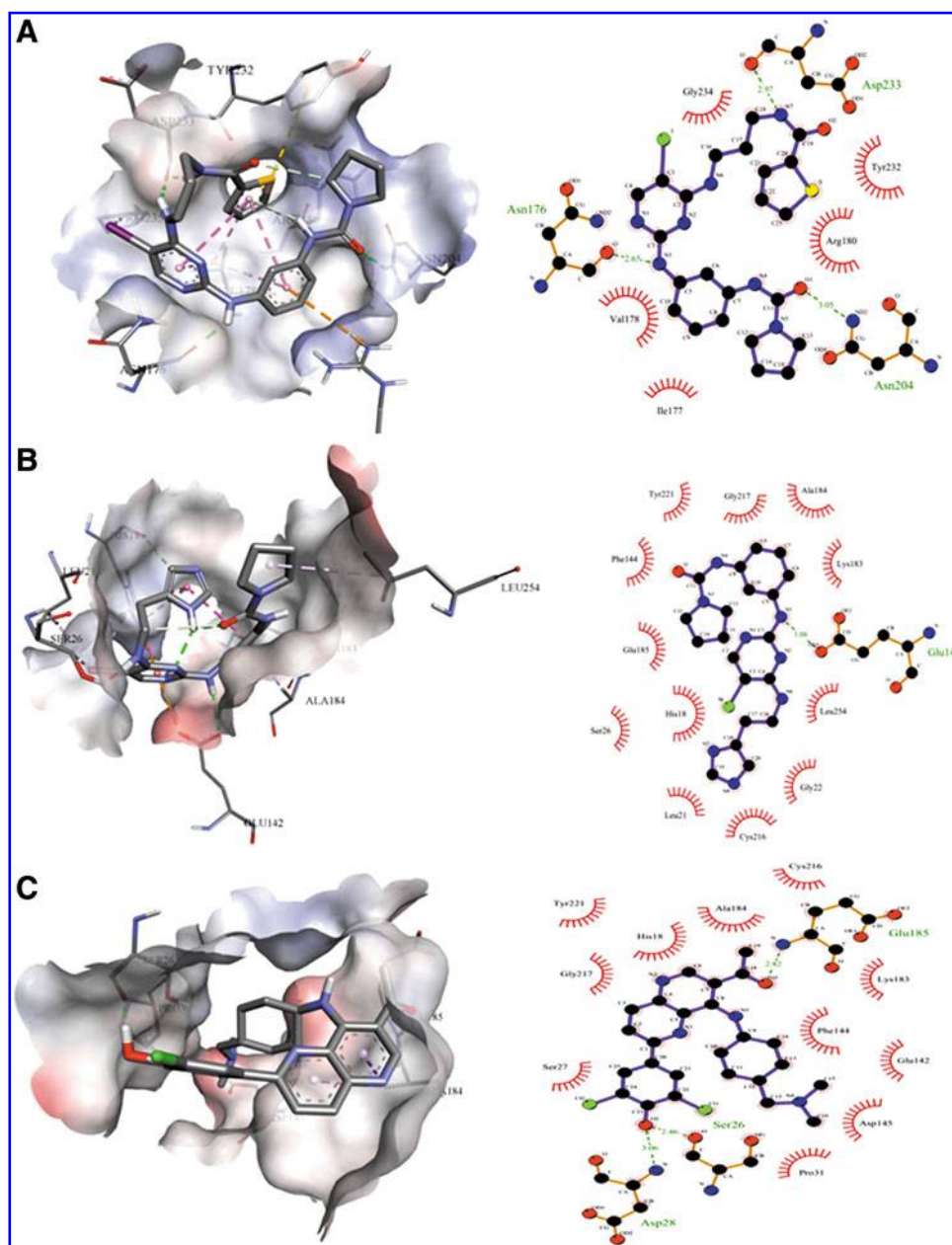


FIG. 1. Overall structure of MARK4-F1 complexed with ligands. Important residues that bind with ligands are shown in *red half circles*, ligands are shown in *blue black dots*. Residues that are form hydrogen bonds are show, in *green color*. (A) BX-795, (B) BX-912, and (C) OTSSP167.

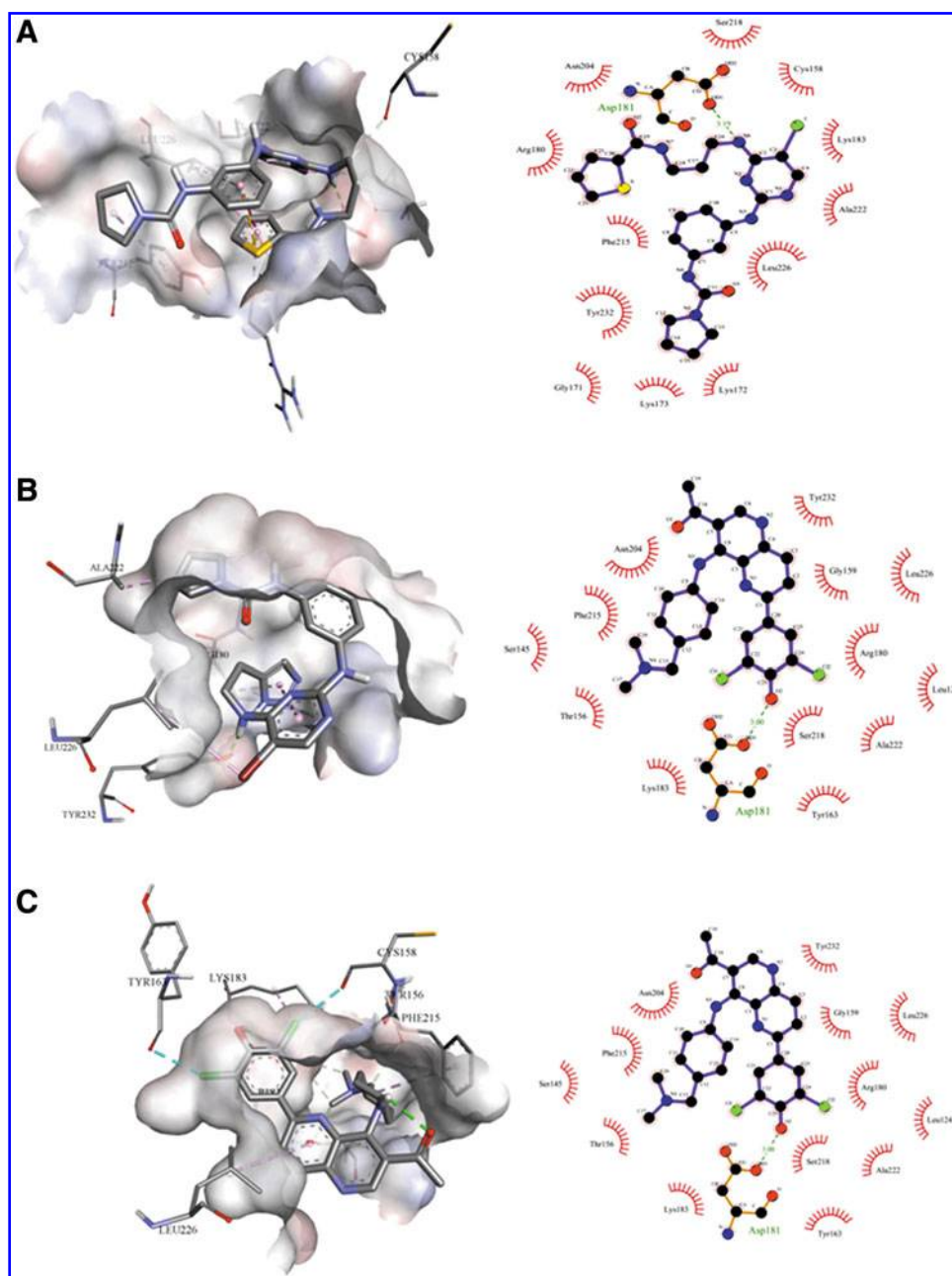


FIG. 2. Overall structure of MARK4-F2 complexed with ligands. Important residues that bind with ligands are shown in *red half circles*, ligands are shown in *blue black dots*. Residues that are form hydrogen bonds are show, in *green color*. (A) BX-795, (B) BX-912, and (C) OTSSP167.

meta-server (Yang et al., 2013) and 3DLigandSiteserver (Wass et al., 2010). All the ligands were docked into the predicted cavities of proteins, and resulted docked conformations were selected on the basis of observed interaction energies and scoring functions. The OTSSP167 showed highest binding free energy to both MARK4-F1 and MARK4-F2 with -7.97 and -7.91 kcal/mol⁻¹, respectively (Table 1).

MD simulations

Selected docked complexes were immersed in the SPC/E water model and minimized in the 700 steps of steepest descent.

Each energetically minimized and solvent equilibrated complex was simulated for 20 ns. GROMACS were used to analyze the behavior of the complexes. The *g_dist* module of GROMACS was used to calculate the distance between the protein and ligands during the course of simulation. The average distance between the MARK4-F1 and ligands, BX-795, BX-912, and OTSSP167 were found to be 1.99 nm, 1.58 nm, and 1.22 nm, respectively. The BX-912 showed relatively higher fluctuations throughout MD simulations, whereas; BX-795 and OTSSP167 showed quite similar behavior (Supplementary Fig. S3).

These results showed that OTSSP167 bound very close to MARK4-F1 as compared to BX-795 and BX-912.

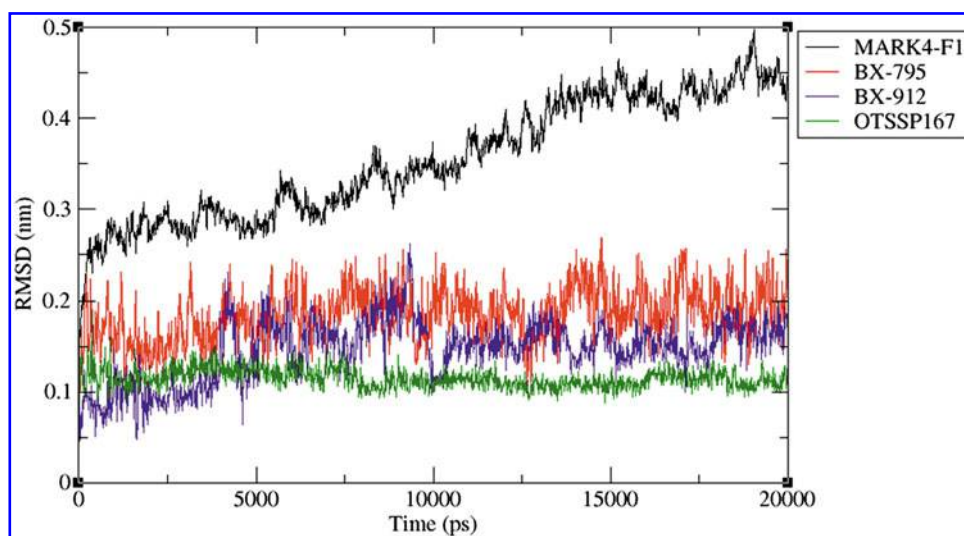


FIG. 3. RMSF plot for MARK4F1 and MARK4F1 complexes.

Hydrogen bonds also showed variations throughout the 20 ns simulations with the average number of such bonds formed by BX-795, BX-912, and OTSSP167 with MARK4-F1, which were found to be 0.51, 1.63, and 2.30, respectively. The number of hydrogen bonds may reach up to six in case of OTSSP167 (Supplementary Fig. S4).

Furthermore, the RMSD value for MARK4-F1 was computed to be 0.35 nm, while values for the ligands BX-795, BX-912, and OTSSP167 were 0.18 nm, 0.14 nm, and 0.11 nm, respectively. OTSSP167 showed relatively lesser variations as compared to rest of the ligands (Fig. 3). These analyses indicate that the complex of MARK4-F1 and OTSSP167 achieved a stable conformation as compared to the rest of the complexes.

Similarly, the distance between the MARK4-F2 and ligands BX-795, BX-912, and OTSSP167 were analyzed and found to be 1.44 nm, 1.12 nm, and 2.7 nm, respectively. The

distance plots for all the ligands showed a continuous variation patterns (Supplementary Fig. S5). The average numbers of hydrogen bond for MARK4-F2 displayed by BX-795, BX-912, and OTSSP167 are 1.64, 2.44, and 0.79, respectively. The number of hydrogen bonds may reach up to six for BX-795 (Supplementary Fig. S6), while for BX-912 and OTSSP167 it is five and four, respectively. The RMSD values were found to be 0.29 nm, 0.12 nm, and 0.18 nm for BX-795, BX-912, and OTSSP167, respectively. OTSSP167 showed the relative stable behavior throughout the course of 20 ns MD simulations (Fig. 4).

Absorption spectra

We have measured absorbance spectra of all three ligands (BX-795, BX-912, and OTSSP167) in the wavelength range of 200 nm to 800 nm (Fig. S7). BX-795 showed

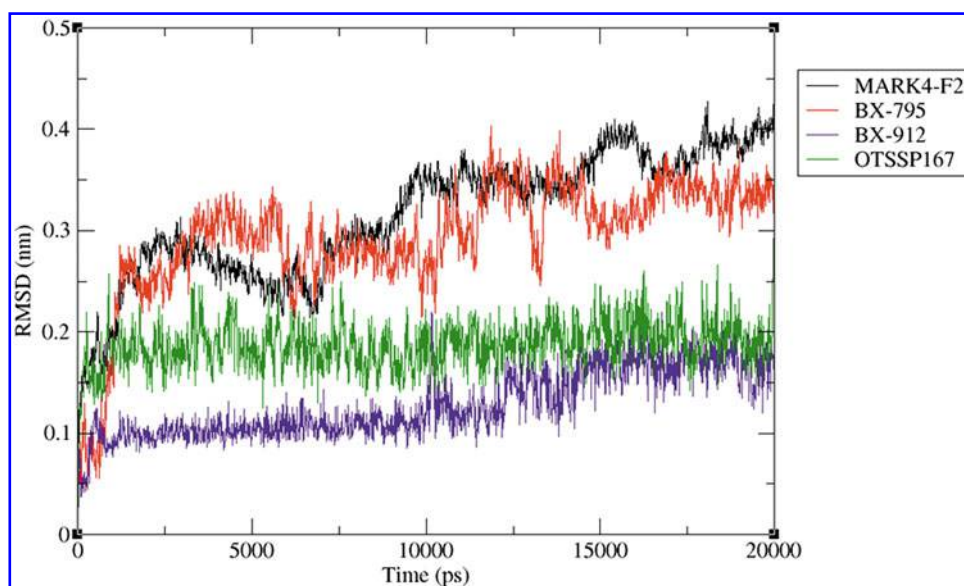


FIG. 4. RMSF plot for MARK4F2 (black), BX-795 (red), BX-912 (violet) and OTSSP167 (green) -MARK4F2-complexes.

λ_{\max} at 232 nm and 372nm; BX-912 showed λ_{\max} at 233nm and 370 nm, and OTSSP167 showed λ_{\max} at 227 nm and 353 nm. From these spectra, we observed that these ligands were not absorbing near 280 nm where proteins absorb. This observation helped us to select the excitation wavelength for fluorescence spectral measurements. As these inhibitors do not absorb near 280 nm, hence we can estimate binding constant of ligands from fluorescence spectra by exciting MARK4 at 280 nm.

Fluorescence study

It is known that a spectral change occurs in the fluorescence emission spectra by successive addition of ligands. A decrease in fluorescence intensity is considered with the formation of stable complex between protein (MARK4) and ligand. This relationship is expressed as,



The association constant K for the above equilibrium is represented by,

$$K = \frac{[\text{complex}]}{[\text{MARK4}][\text{ligand}]} \quad (\text{Eq. 2})$$

Here MARK4 is either MARK4-F1 or MARK4-F2, K is the binding constant, and n is the number of binding sites.

The fluorescence emission spectra of the buffer with increasing concentrations of ligands were taken for baseline correction (Supplementary Fig. S8 A, B, C). Fluorescence emission spectra of protein were also taken with increasing concentration of buffer in order to nullify the effect of the buffer (Supplementary Fig. S9 A, B). With the increasing concentration of all three ligands BX-795, BX-912, and OTSSP167, a decrease in fluorescence emission was observed for both MARK4-F1 and MARK4-F2. This quenching in fluorescence was used to calculate the binding constant K for each ligands to the MARK4.

For these studies, solutions containing 0.1 mg/ml of MARK4-F1 and MARK4-F2 were taken and increasing amount of each ligand was added to both the proteins. Supplementary Figures S10 and S11 represent the fluorescence emission spectra of MARK4-F1 and MARK4-F2, respectively. All spectra were corrected for baseline with the corresponding amount of ligands and buffer in the presence of different concentrations of ligands at 25°C.

The typical emission peak was observed at λ_{\max} 343 for MARK4-F1 and λ_{\max} 342 for MARK4-F2. It can be seen that the fluorescence intensity at 343 and 342 nm decreases with addition of ligands. This change in fluorescence intensity at 343 and 342 nm was used to estimate K and n for the binding of inhibitors to MARK4-F1 and MARK4-F2 using the relation (Barik et al., 2003; Feng et al., 1998),

$$\text{Log}(F_0 - F)/F = \text{log}K_b + n\text{log}[\text{ligand}] \quad (\text{Eq. 3})$$

Here, F_0 and F are value of fluorescence intensity of the fluorophore (MARK4-F1 and MARK4-F2) at 342 nm and 342 nm in the absence and the presence of different concentrations of ligand, respectively. Figures 5 and 6 show a

linear plot for $(\log (F_0 - F)/F)$ versus $\log [\text{ligand}]$ for MARK4-F1 and MARK4-F2, respectively.

According to Equation 3, the values of K were estimated to be $2.4 \times 10^4 \text{ M}^{-1}$ (MARK4-F1) and $3.3 \times 10^4 \text{ M}^{-1}$ (MARK4-F2) for BX-795, $3.7 \times 10^3 \text{ M}^{-1}$ (MARK4-F1) and $7.13 \times 10^3 \text{ M}^{-1}$ (MARK4-F2) for BX-912, and $3.9 \times 10^3 \text{ M}^{-1}$ (MARK4-F1), and $1.9 \times 10^3 \text{ M}^{-1}$ (MARK4-F2) for OTSSP167 (Table. 2). The number of binding sites were 0.87 (MARK4-F1) and 0.92 (MARK4-F2) for BX-795, 0.75 (MARK4-F1) and 0.82 (MARK4-F2) for BX-912, and 0.67 (MARK4-F1) and 0.63 (MARK4-F2) for OTSSP167. These measurements suggested that there is a single binding site for all the three ligands to both types of MARK4.

Discussion

MARK4 plays a crucial role in cellular pathways, and its abnormal phosphorylation activity is directly linked with

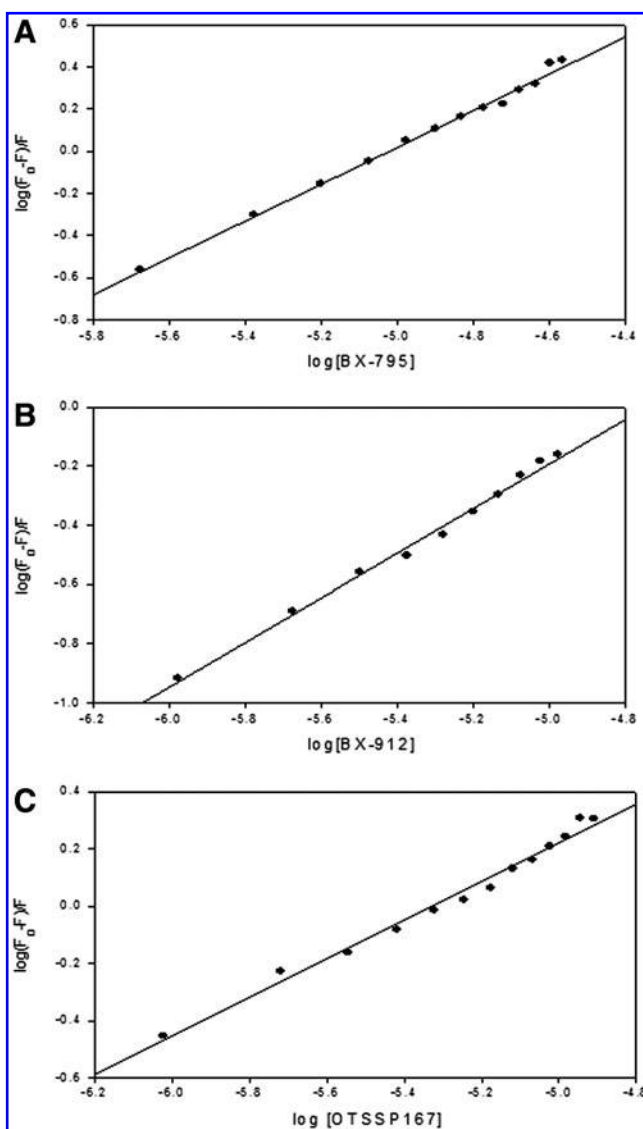


FIG. 5. Linear plot for $\log (F_0 - F)/F$ vs. $\log [\text{ligands}]$ of MARKF1 according to Equation (4). (A) BX-795, (B) BX-912, and (C) OTSSP167.

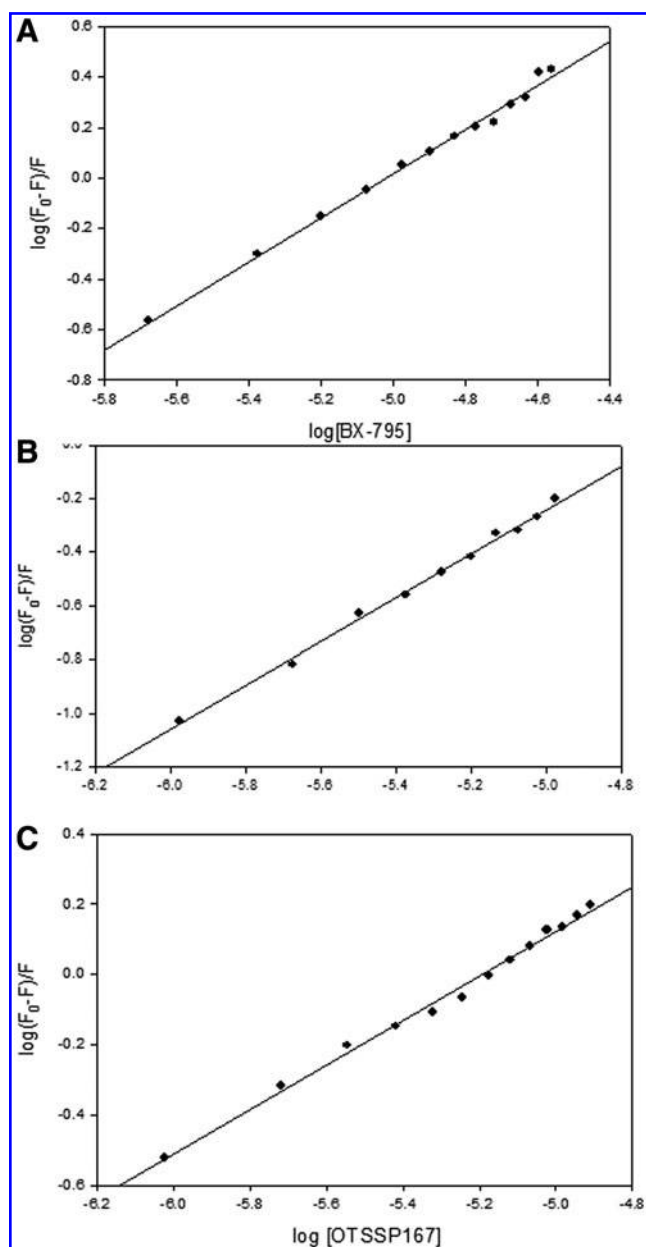


FIG. 6. Linear plot for $\log(F_0-F)/F$ vs. $\log[\text{ligands}]$ of MARK4F2 according to Equation (4). (A) BX-795, (B) BX-912, and (C) OTSSP167.

TABLE 2. DIFFERENT PARAMETERS OBTAINED FROM FLUORESCENCE SPECTROSCOPIC LIGAND BINDING STUDIES FOR MARK4

Ligand	Parameter	MARK4F1	MARK4F2
BX-795	K_a	$2.4 \times 10^4 \text{ M}^{-1}$	$3.3 \times 10^4 \text{ M}^{-1}$
	n	0.87	0.92
	K_D	$6.46 \mu\text{M}$	$9.74 \mu\text{M}$
BX-912	K_a	$3.7 \times 10^3 \text{ M}^{-1}$	$7.13 \times 10^3 \text{ M}^{-1}$
	n	0.75	0.82
	K_D	$4.11 \mu\text{M}$	$5.90 \mu\text{M}$
OTSSP167 (hydrochloride)	K_a	$3.9 \times 10^3 \text{ M}^{-1}$	$1.9 \times 10^3 \text{ M}^{-1}$
	n	0.67	0.63
	K_D	$1.7 \mu\text{M}$	$1.8 \mu\text{M}$

various human disorders, including cancer, type2 diabetes, obesity, metabolic disorders, and neurodegenerative disorders (Naz et al., 2013, 2015a). Therefore, modulation of kinase activity of MARK4 using potent inhibitorS may be an attractive strategy for the treatment of associated disorders. A combined molecular docking and MD simulation studies were carried out to understand the structural bases of MARK4 inhibition. These *in silico* studies were further validated by fluorescence studies that clearly indicate a significant binding affinity of three ligands BX-795, BX-912, and OTSSP167 to the MARK4.

A combination of computational study with experiments is the best way for the structure-based drug design and discovery (Hoda et al., 2015). Recent advances in the field of computational biology have resulted in deciphering important clues that leads to discovery of novel drugs against several diseases (Aneja et al., 2015, Shahbaaz et al., 2015a, b).

Sialidase activity of *Porphyromonas gingivalis* has been implicated in the onset of periodontitis. Structural study of sialidase β -propeller domain of *P. gingivalis* has shown that alteration in salt bridge formation within this domain leads to change in the sialidase activity, and thus may lead to potential treatment against peridontitis (Cueno et al., 2014).

In another study, a computational approach helped to identify 11 anti-diabetic medicinal plants (Sahu et al., 2014). These markers may be helpful in the identification of plants with anti-diabetic property in the future and reflect the importance of computational approaches in the identification of biomarkers and novel therapeutics against emerging diseases.

Our docking studies indicate a significant complexation of all three ligands to the MARK4. We found that OTSSP167 inhibits both MARK4-F1 and MARK4-F2 more efficiently than the other ligands. The OTSSP167 interacts with His18, Ser27, Pro31, Glu142, Phe144, Asp145, Lys183, Ala184, Glu185, Cys216, Gly217, and Tyr221 of MARK4-F1 (Fig. 1C). In MARK4-F2, it shows interaction with Leu124, Ser145, Thr156, Gly159, Tyr163, Arg180, Asp181, Lys183, Asn204, Phe215, Ser218, Ala222, Leu226, and Tyr232 (Fig. 2C).

These reactions were correlated with the previous findings, in which the crystal structure of OTSSP 167 with MPK38 (PDB ID-4CQG) has been published (Cho et al., 2014). They also shown that OTSSP 167 efficiently inhibits the activity of the MPK38 by binding to its active site, which was indicated by the interaction studies and its IC_{50} value measurement (Cho et al., 2014). It was recently reported that OTSSP167, the MELK selective inhibitor, effectively suppresses MELK kinase activity, with an IC_{50} of 0.41 nM (Chung et al., 2012). The present study helps better understanding of the binding mode of the MARK4 inhibitor and provides a foundation for structure-guided drug design.

In the case of MARK4-F2, all ligands showed a conserved pattern of interacting residues (i.e., Arg180, Asp181, Lys183, Asn204, Phe215, Ser218, Ala222, Leu226, and Tyr232 (Fig. 2A–C), indicating that these residues are important for the binding with either ligands or substrates. Among them, Asp181 is the active site residue of MARK4, which also interacts with these ligands. By blocking this site with

inhibitors, ATP will not be able to bind with MARK4. Ser218 is an important phosphorylation site of MARK4. OTSSP167 forms three hydrogen bonds with MARK4-F1 (Ser26: 2.46 Å, Asp28: 3.06 Å, and Glu185: 2.82 Å) and one hydrogen bond with MARK4-F2 (Asp181: 3.0 Å).

Hydrogen bonds and interacting residues are illustrated in Figures 1 and 2. OTSSP167 showed highest free energy of binding, indicating a best inhibitor (Table 1). After MD simulation, we have observed the same results that OTSSP167 showed relatively stable parameters for the MARK4-F1 protein, while all other ligands were showing quite similar behavior for MARK4-F2 protein.

We have also determined the dissociation constant (K_D) of the MARK4-F1 and MARK4-F2 for all three ligands based on the David Sheehan method using Equation 5 (Sheehan, 2009). Changes in intrinsic fluorescence (ΔF) as a result of ligand binding to MARK4-F1 and MARK4-F2 were determined. Plots of $1/\Delta F$ versus $1/[\text{ligand}]$ are linear (Figs. 7 and 8). The K_D was determined from the intercept of the line

on the abscissa. Values of calculated K_D for MARK4-F1 and MARK4-F2 are given in Table 2.



$$K_D = \frac{[\text{MARK4}][\text{ligand}]}{[\text{complex}]} \quad (\text{Eq. 5})$$

here, K_D is a measure of the affinity of the MARK4 for the ligand.

Basically, intrinsic fluorescence of any protein including MARK4 is almost due to tryptophan because tyrosine fluorescence is quenched by tryptophan resulting in a very low

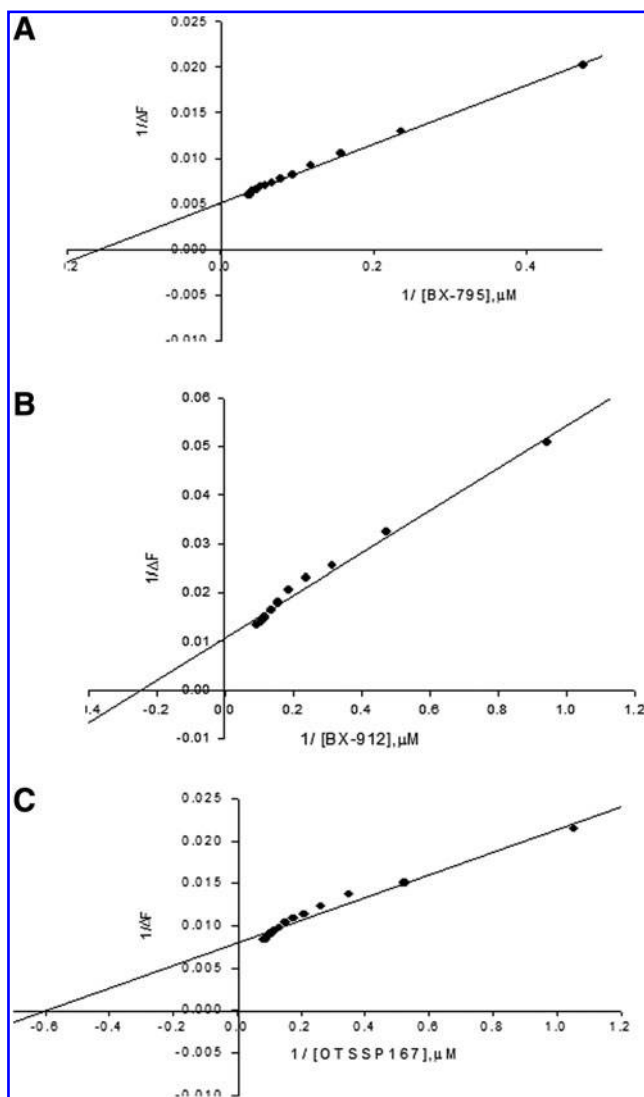


FIG. 7. Linear plot for $\log(F_0 - F)/F$ vs. $\log[\text{ligands}]$ of MARK4-F1 according to Equation (4). (A) BX-795, (B) BX-912, and (C) OTSSP167.

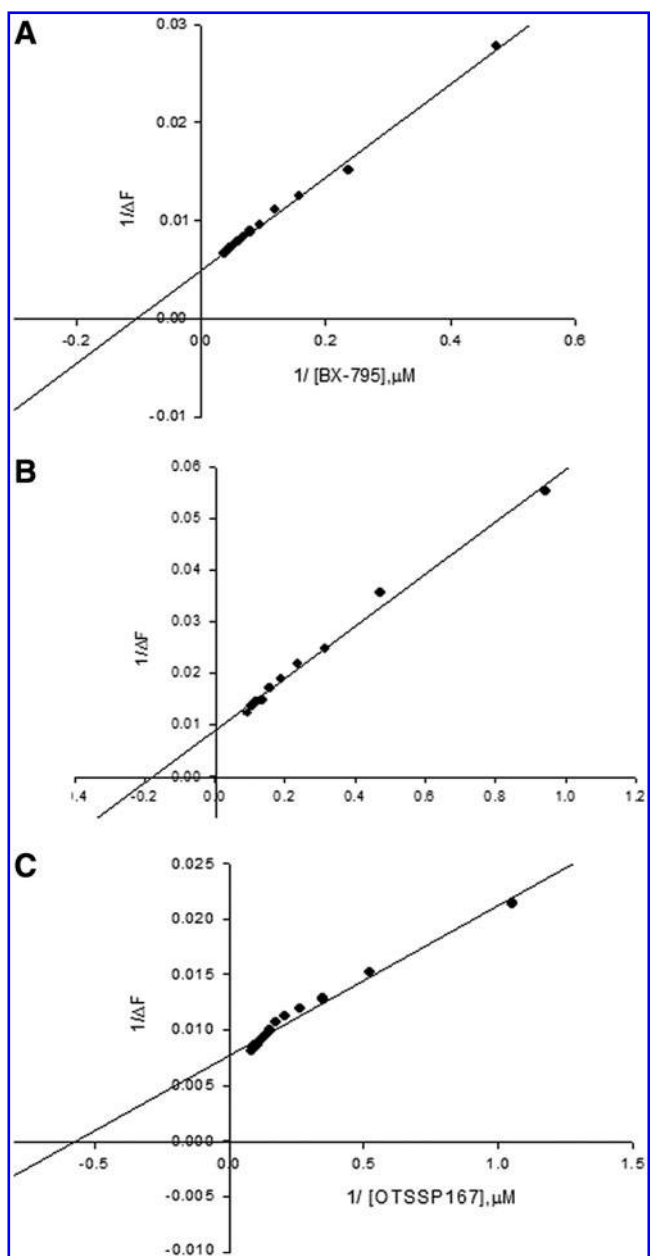


FIG. 8. Linear plot for $\log(F_0 - F)/F$ vs. $\log[\text{ligands}]$ of MARK4-F2 according to Equation (4). (A) BX-795, (B) BX-912, and (C) OTSSP167.

quantum yield (Eftink and Ghiron, 1981; Zhang et al., 2006). Hence, changeS in the intrinsic fluorescence intensity of MARK4-F1 and MARK4-F2 were observed due to the tryptophan residue when ligands bind. A decrease in the fluorescence emission is an indication of ligand binding to the protein molecule.

All these observations clearly indicate that OTSSP167 showed better specificity and binding affinity with MARK4 via forming a stable interaction with key residues. Structure analysis also suggests that closure of the catalytic cleft observed in the ligand bound complexes and its independency to the movement of the T-loop makes them promising candidates in hampering the role of MARK4 in various diseases. Thus, its derivatives can be used as therapeutic target against various life-threatening diseases.

Conclusions

In this study, we demonstrate the role of significant residues of MARK4 that help in the substrate/inhibitor binding. We further explored finding some efficient ligand whose derivatives can be used as therapeutic agent for MARK4 associated diseases. The molecular docking approach combined with experimental studies suggests that OTSSP167 has highest binding-affinity to the MARK4 as compared to other ligands. Hence, OTSSP167 may be a potential inhibitor for both the MARK4-F1 and MARK4-F2 proteins.

These studies will be helpful for the identification of potent MARK4 inhibitors with appropriate target selectivity, cellular efficacy, therapeutic effectiveness, and tolerability with novel pharmacophore features. Finally, this work gives information about the formation of a stable complex (ligand-MARK4), which opens a new promising avenue towards the application of these ligands and their derivatives for the treatment of ailments associated with MARK4. Further optimizations are called for.

Acknowledgments

FN acknowledges the Council of Scientific and Industrial Research for the award of fellowship. We thank Dana-Farber/Harvard Cancer Center (DF/HCC) Boston, MA, for providing the clone of MARK4. FA and MIH are thankful to the Department of Science and Technology (Government of India) and Indian Council for Medical Research (ICMR) for financial support. The authors thank Department of Science and Technology, Government of India for FIST support (SR/FST/LSI-541/2012).

Author Disclosure Statement

The authors declare they have no conflicting financial interests.

References

Altschul SF, Gish W, Miller W, et al. (1990). Basic local alignment search tool. *J Mol Biol* 215, 403–410.

Aneja B, Irfan M, Hassan MI, et al. (2015). Monocyclic beta-lactam and unexpected oxazinone formation: Synthesis, crystal structure, docking studies and antibacterial evaluation. *J Enzyme Inhib Med Chem* 1–19.

Bain J, Plater L, Elliott M, et al. (2007). The selectivity of protein kinase inhibitors: A further update. *Biochem J* 408, 297–315.

Barik A, Priyadarsini KI, and Mohan H. (2003). Photophysical studies on binding of curcumin to bovine serum albumins. *Photochem Photobiol* 77, 597–603.

BIOVIA DS. (2013). *Discovery Studio Modeling Environment*. San Diego: Dassault Systèmes.

Bright NJ, Thornton C, and Carling D. (2009). The regulation and function of mammalian AMPK-related kinases. *Acta Physiol (Oxf)* 196, 15–26.

Brognaard J, and Hunter T. (2011). Protein kinase signaling networks in cancer. *Curr Opin Genet Dev* 21, 4–11.

Cho YS, Kang Y, Kim K, et al. (2014). The crystal structure of MPK38 in complex with OTSSP167, an orally administrative MELK selective inhibitor. *Biochem Biophys Res Commun* 447, 7–11.

Chung S, Suzuki H, Miyamoto T, et al. (2012). Development of an orally-administrative MELK-targeting inhibitor that suppresses the growth of various types of human cancer. *Oncotarget* 3, 1629–1640.

Clark K, Plate L, Pegg M, and Cohen P. (2009). Use of the pharmacological inhibitor BX795 to study the regulation and physiological roles of TBK1 and IkappaB kinase epsilon: A distinct upstream kinase mediates Ser-172 phosphorylation and activation. *J Biol Chem* 284, 14136–14146.

Conrad F, Zhu X, Zhang X, et al. (2009). Human antibodies targeting cell surface antigens overexpressed by the hormone refractory metastatic prostate cancer cells: ICAM-1 is a tumor antigen that mediates prostate cancer cell invasion. *J Mol Med (Berl)* 87, 507–514.

Cowan-Jacob SW, Mobitz H, and Fabbro D. (2009). Structural biology contributions to tyrosine kinase drug discovery. *Curr Opin Cell Biol* 21, 280–287.

Cueno ME, Kamio N, Imai K, et al. (2014). Structural significance of the beta1K396 residue found in the Porphyromonas gingivalis sialidase beta-propeller domain: A computational study with implications for novel therapeutics against periodontal disease. *OMICS* 18, 591–599.

Dimitrakopoulou K, Dimitrakopoulos GN, Sgarbas KN, and Bezerianos A. (2014). Tamoxifen integromics and personalized medicine: Dynamic modular transformations underpinning response to tamoxifen in breast cancer treatment. *OMICS* 18, 15–33.

Drewes G, Ebnet A, Preuss U, et al. (1997). MARK, a novel family of protein kinases that phosphorylate microtubule-associated proteins and trigger microtubule disruption. *Cell* 89, 297–308.

Drewes G, Trinczek B, Illenberger S, et al. (1995). Microtubule-associated protein/microtubule affinity-regulating kinase (p110mark). A novel protein kinase that regulates tau-microtubule interactions and dynamic instability by phosphorylation at the Alzheimer-specific site serine 262. *J Biol Chem* 270, 7679–7688.

Eftink MR, and Ghiron CA. (1981). Fluorescence quenching studies with proteins. *Anal Biochem* 114, 199–227.

Eswar N, Webb B, Marti-Renom, MA, Madhusudhan MS, et al. (2006). Comparative protein structure modeling using Modeller. *Curr Protoc Bioinformatics* Chapter 5, Unit 5 6.

Feldman RI, Wu JM, Polokoff MA, et al. (2005). Novel small molecule inhibitors of 3-phosphoinositide-dependent kinase-1. *J Biol Chem* 280, 19867–19874.

Feng XZ, Lin Z, Yang LJ, et al. (1998). Investigation of the interaction between acridine orange and bovine serum albumin. *Talanta* 47, 1223–1229.

Gabrovskva PN, Smith RA, Tiang T, Weinstein SR, et al. (2012). Development of an eight gene expression profile implicat-

- ing human breast tumours of all grade. *Mol Biol Rep* 39, 3879–3892.
- Gray D, Jubb AM, Hogue D, Dowd P, et al. (2005). Maternal embryonic leucine zipper kinase/murine protein serine-threonine kinase 38 is a promising therapeutic target for multiple cancers. *Cancer Res* 65, 9751–9761.
- Hassan M, Kumar V, Somvanshi RK, et al. (2007a). Structure-guided design of peptidic ligand for human prostate specific antigen. *J Peptide Sci* 13, 849–855.
- Hassan MI, Kumar V, Singh TP, and Yadav S. (2007b). Structural model of human PSA: A target for prostate cancer therapy. *Chem Biol Drug Des* 70, 261–267.
- Hirashima A, and Huang H. (2008). Homology modeling, agonist binding site identification, and docking in octopamine receptor of *Periplaneta americana*. *Comput Biol Chem* 32, 185–190.
- Hoda N, Naz H, Jameel E, et al. (2015). Curcumin specifically binds to the human calcium-calmodulin-dependent protein kinase IV: Fluorescence and molecular dynamics simulation studies. *J Biomol Struct Dyn* 1–13.
- Holm L, and Rosenstrom P. (2010). Dali server: Conservation mapping in 3D. *Nucleic Acids Res* 38, W545–549.
- Illenberger S, Drewes G, Trinczek B, et al. (1996). Phosphorylation of microtubule-associated proteins MAP2 and MAP4 by the protein kinase p110mark. Phosphorylation sites and regulation of microtubule dynamics. *J Biol Chem* 271, 10834–10843.
- Jiang P, and Zhang D. (2013). Maternal embryonic leucine zipper kinase (MELK): A novel regulator in cell cycle control, embryonic development, and cancer. *Int J Mol Sci* 14, 21551–21560.
- Joshi K, Banasavadi-Siddegowda Y, Mo X, et al. (2013). MELK-dependent FOXM1 phosphorylation is essential for proliferation of glioma stem cells. *Stem Cells* 31, 1051–1063.
- Kato T, Satoh S, Okabe H, et al., (2001). Isolation of a novel human gene, MARKL1, homologous to MARK3 and its involvement in hepatocellular carcinogenesis. *Neoplasia* 3, 4–9.
- Kemphues K. (2000). PARsing embryonic polarity. *Cell* 101, 345–348.
- Kloo B, Nagel D, Pfeifer M, et al. (2011). Critical role of PI3K signaling for NF-kappaB-dependent survival in a subset of activated B-cell-like diffuse large B-cell lymphoma cells. *Proc Natl Acad Sci USA* 108, 272–277.
- Laskowski RA, Rullmannn JA, MacArthur MW, et al. (1996). AQUA and PROCHECK-NMR: Programs for checking the quality of protein structures solved by NMR. *J Biomol NMR* 8, 477–486.
- Lewis J, Lipworth W, and Kerridge I. (2014). Ethics, evidence and economics in the pursuit of “personalized medicine”. *J Pers Med* 4, 137–146.
- Li L, and Guan KL. (2013). Microtubule-associated protein/microtubule affinity-regulating kinase 4 (MARK4) is a negative regulator of the mammalian target of rapamycin complex 1 (mTORC1). *J Biol Chem* 288, 703–708.
- Magnani I, Novielli, C, Fontana, L, et al. (2011). Differential signature of the centrosomal MARK4 isoforms in glioma. *Anal Cell Pathol (Amst)* 34, 319–338.
- Marx A, Nugoore C, Panneerselvam S, and Mandelkow E. (2010). Structure and function of polarity-inducing kinase family MARK/Par-1 within the branch of AMPK/Snf1-related kinases. *FASEB J* 24, 1637–1648.
- Mashukova A, Forteza R, Wald FA, and Salas PJ. (2012). PDK1 in apical signaling endosomes participates in the rescue of the polarity complex atypical PKC by intermediate filaments in intestinal epithelia. *Mol Biol Cell* 23, 1664–1674.
- Morris GM, Huey R, Lindstrom W, et al., (2009). AutoDock4 and AutoDockTools4: Automated docking with selective receptor flexibility. *J Comput Chem* 30, 2785–2791.
- Nakano I, Joshi K, Visnyei K, et al. (2011). Siomycin A targets brain tumor stem cells partially through a MELK-mediated pathway. *Neuro Oncol* 13, 622–634.
- Naz F, Anjum F, Islam A, et al. (2013). Microtubule affinity-regulating kinase 4: Structure, function, and regulation. *Cell Biochem Biophys* 67, 485–499.
- Naz F, Asad M, Malhotra P, et al., (2014). Cloning, expression, purification and refolding of microtubule affinity-regulating kinase 4 expressed in *Escherichia coli*. *Appl Biochem Biotechnol* 172, 2838–2848.
- Naz F, Islam A, Ahmad F, and Hassan MI. (2015a). Atypical PKC phosphorylates microtubule affinity-regulating kinase 4 in vitro. *Mol Cell Biochem (in press)*. DOI: 10.1007/s11010-015-2555-3.
- Naz F, Singh P, Islam A, et al. (2015b). Human microtubule affinity-regulating kinase 4 is stable at extremes of pH. *J Biomol Struct Dyn (in press)*. DOI: 10.1080/07391102.2015.1074942.
- Neudert G, and Klebe G. (2011). DSX: A knowledge-based scoring function for the assessment of protein-ligand complexes. *J Chem Inf Model* 51, 2731–2745.
- Oostenbrink C, Villa A, Mark AE, and van Gunsteren WF. (2004). A biomolecular force field based on the free enthalpy of hydration and solvation: The GROMOS force-field parameter sets 53A5 and 53A6. *J Comput Chem* 25, 1656–1676.
- Pace CN, Vajdos F, Fee L, et al. (1995). How to measure and predict the molar absorption coefficient of a protein. *Protein Sci* 4, 2411–2423.
- Peifer C, and Alessi DR. (2008). Small-molecule inhibitors of PDK1. *ChemMedChem* 3, 1810–1838.
- Pronk S, Pall S, Schulz R, et al. (2013). GROMACS 4.5: A high-throughput and highly parallel open source molecular simulation toolkit. *Bioinformatics* 29, 845–854.
- Sahu J, Sen P, Choudhury MD, et al., (2014). Rediscovering medicinal plants’ potential with OMICS: Microsatellite survey in expressed sequence tags of eleven traditional plants with potent antidiabetic properties. *OMICS* 18, 298–309.
- Schuttelkopf AW, and van Aalten DM. (2004). PRODRG: A tool for high-throughput crystallography of protein-ligand complexes. *Acta Crystallogr D Biol Crystallogr* 60, 1355–1363.
- Shahbaaz M, Bisetty K, Ahmad F, and Hassan MI. (2015a). Current advances in the identification and characterization of putative drug and vaccine targets in the bacterial genomes. *Curr Top Med Chem (in press)*.
- Shahbaaz M, Bisetty, K, Ahmad, F, and Hassan, MI. (2015b). Towards New Drug Targets? Function Prediction of Putative Proteins of *Neisseria meningitidis* MC58 and Their Virulence Characterization. *OMICS* 19, 416–434.
- Sheehan D. 2009. Physical biochemistry : principles and applications. 2nd edition. Wiley-Blackwell, Chichester, UK ; Hoboken, NJ.
- Shibata E, Kanno, T, Tsuchiya, A, Kuribayashi, K, et al., (2013). Free fatty acids inhibit protein tyrosine phosphatase 1B and activate Akt. *Cell Physiol Biochem* 32, 871–879.
- Siddique YH, Naz, F, Jyoti, S, Fatima, A, et al., (2014). Effect of *Centella asiatica* Leaf Extract on the Dietary Supplementation in Transgenic *Drosophila* Model of Parkinson’s Disease. *Parkinsons Dis* 2014, 262058.
- Singh A, Kumar Thakur, P, Meena, M, Kumar, D, et al., (2014). Interaction between Basic 7S Globulin and Leguminin in

- Soybean [Glycine max]: A Structural Insight. *Letters in Drug Design & Discovery* 11, 231–239.
- Sun C, Tian, L, Nie, J, Zhang, H, et al., (2012). Inactivation of MARK4, an AMP-activated protein kinase (AMPK)-related kinase, leads to insulin hypersensitivity and resistance to diet-induced obesity. *J Biol Chem* 287, 38305–38315.
- Tamguney T, Zhang, C, Fiedler, D, Shokat, K, et al., (2008). Analysis of 3-phosphoinositide-dependent kinase-1 signaling and function in ES cells. *Exp Cell Res* 314, 2299–2312.
- Tang EI, Xiao, X, Mruk, DD, Qian, XJ, et al., (2012). Microtubule affinity-regulating kinase 4 (MARK4) is a component of the ectoplasmic specialization in the rat testis. *Spermatogenesis* 2, 117–126.
- Thakur PK and Hassan, I. (2011). Discovering a potent small molecule inhibitor for gankyrin using de novo drug design approach. *Int J Comput Biol Drug Des* 4, 373–386.
- Thakur PK, Prakash, A, Khan, P, Fleming, RE, et al., (2013). Identification of Interfacial Residues Involved in Hepcidin-Ferroportin Interaction. *Lett Drug Des Discov* 11, 363–374.
- Timm T, Marx, A, Panneerselvam, S, Mandelkow, E, et al., (2008). Structure and regulation of MARK, a kinase involved in abnormal phosphorylation of Tau protein. *BMC Neurosci* 9 Suppl 2, S9.
- Trinczek B, Brajenovic, M, Ebneith, A, and Drewes, G. (2004). MARK4 is a novel microtubule-associated proteins/microtubule affinity-regulating kinase that binds to the cellular microtubule network and to centrosomes. *J Biol Chem* 279, 5915–5923.
- Vanommeslaeghe K, Hatcher, E, Acharya, C, Kundu, S, et al., (2010). CHARMM general force field: A force field for drug-like molecules compatible with the CHARMM all-atom additive biological force fields. *J Comput Chem* 31, 671–690.
- Wallner B and Elofsson, A. (2003). Can correct protein models be identified? *Protein Sci* 12, 1073–1086.
- Wass MN, Kelley, LA, and Sternberg, MJ. (2010). 3DLi-gandSite: predicting ligand-binding sites using similar structures. *Nucleic Acids Res* 38, W469–473.
- Yang J, Roy, A, and Zhang, Y. (2013). Protein-ligand binding site recognition using complementary binding-specific sub-structure comparison and sequence profile alignment. *Bioinformatics* 29, 2588–2595.
- Yesilkanal AE and Rosner, MR. (2014). Raf kinase inhibitory protein (RKIP) as a metastasis suppressor: regulation of signaling networks in cancer. *Crit Rev Oncog* 19, 447–454.
- Zhang J, Yang, PL, and Gray, NS. (2009). Targeting cancer with small molecule kinase inhibitors. *Nat Rev Cancer* 9, 28–39.
- Zhang L, Kao, YT, Qiu, W, Wang, L, et al., (2006). Femtosecond studies of tryptophan fluorescence dynamics in proteins: local solvation and electronic quenching. *J Phys Chem B* 110, 18097–18103.
- Zielkiewicz J. (2005). Structural properties of water: comparison of the SPC, SPCE, TIP4P, and TIP5P models of water. *J Chem Phys* 123, 104501.

Address correspondence to:

Md. Imtaiyaz Hassan, PhD

Centre for Interdisciplinary Research in Basic Sciences

Jamia Millia Islamia

Jamia Nagar

New Delhi 110025

India

E-mail: mihassan@jmi.ac.in

This article has been cited by:

1. Shikha Kumari, Danish Idrees, Chandra Bhushan Mishra, Amresh Prakash, Wahiduzzaman, Faizan Ahmad, Md. Imtaiyaz Hassan, Manisha Tiwari. 2016. Design and synthesis of a novel class of carbonic anhydrase-IX inhibitor 1-(3-(phenyl/4-fluorophenyl)-7-imino-3H-[1,2,3]triazolo[4,5d]pyrimidin 6(7H)y)urea. *Journal of Molecular Graphics and Modelling* **64**, 101-109. [[CrossRef](#)]
2. Shama Khan, Mohd. Shahbaaz, Krishna Bisetty, Faizan Ahmad, Md. Imtaiyaz Hassan. 2015. Classification and Functional Analyses of Putative Conserved Proteins from Chlamydomonada pneumoniae CWL029. *Interdisciplinary Sciences: Computational Life Sciences* . [[CrossRef](#)]
3. Farha Naz, Mohd. Shahbaaz, Shama Khan, Krishna Bisetty, Asimul Islam, Faizan Ahmad, Md. Imtaiyaz Hassan. 2015. PKR-inhibitor binds efficiently with human microtubule affinity-regulating kinase 4. *Journal of Molecular Graphics and Modelling* **62**, 245-252. [[CrossRef](#)]